SEMARAK ILMU PUBLISHING

Journal of Advanced Research in Applied Mechanics

Journal homepage:
https://semarakilmu.com.my/journals/index.php/appl_mech/index
ISSN: 2289-7895

The Novel Method in Validating the Spectral Wavelength Optimization to Determine Archaeological Proxies by the Integration of Aerial and Ground Platforms

Shairatul Akma Roslan[1,*], Fitri Yakub[1], Shuib Rambat[1], Sharifah Munawwarah[2], Mokhtar Saidin[3], Farah Liana[1], Nurshafinaz Mohd Maruai[1], Mohamed Sukri Mat Ali[1], Ahmad Faiz Mohammad[1]

[1] Malaysia–Japan International Institute of Technology (MJIIT), Universiti Teknologi Malaysia, Jalan Sultan Yahya Petra, 54100 Kuala Lumpur, Malaysia
[2] Faculty of Systems and Information Engineering, University of Tsukuba, Tsukuba 305-8573, Japan
[3] Centre for Global Archaeology Research (CGAR), Universiti Sains Malaysia, 11800 Pulau Pinang, Malaysia

ARTICLE INFO

Article history:
Received 3 April 2023
Received in revised form 9 june 2023
Accepted 16 June 2023
Available online 1 July 2023

Keywords:
CEE method; optimal spectral; vegetation indices; spectral analysis remote sensing; geophysical

ABSTRACT

This research proposed a novel method for evaluating the ideal spectral wavelength by integrating the aerial remote sensing image and geophysical techniques to improve the detection of buried archaeological proxies via the spectral wavelength. Eight different wavelength ranges were compared to eight distinct spectral indices to conduct a more thorough vegetation analysis. The spectral information from eight various Vegetation Indices and two types of resistivity data was then analyzed using a Linear Regression model. Then, the novel "Constant Experimental Evaluation" method (CEE) was developed to improve the preliminary result. Subsequently, the results outlined newly optimal spectral wavelengths by enhancing correlation coefficient R^2 values, before (R^2=0.595) to (R^2=0.86) after CEE application, with the spectral wavelengths values of (NIR_{new}=0.783µm) and (Red_{new}=0.627µm) along with the 50% of image enhancement. It suggests that the technique may be significant to any archaeological site that presents spectrally differently from its immediate environment.

1. Introduction

The accessibility and efficiency of technology have witnessed a revolutionary transition in recent years, providing a bewildering variety of new possibilities for finding and understanding archaeological landscapes. Researchers in archaeology and other disciplines have profited immensely by using aerial remote sensing and ground geophysical approaches in their exploration and study thanks to these advancements [1–5]. Optical imaging, thermal, and radar remote sensing instruments have all been used extensively to map and monitor archaeological sites [6, 7]. Notably, images obtained by remote sensing are also constructed by using spatial, spectral, radiometric, and temporal resolutions [8–11]. Meanwhile, ground geophysical prospection has aided in cutting-edge

* *Corresponding author.*
E-mail address: saroslan@graduate.utm.my

https://doi.org/10.37934/aram.108.1.115

surveys and studies that have expanded beyond geophysics and geology to incorporate the archaeological context at a new scale. Studies [12] have claimed that geophysical and remote sensing technologies are non-invasive, cost-effective, and offer a flexible and alternative means of exploring and defining underlying structures. For instance, combining multiple remote sensing datasets with the ground geophysical investigation has proven to be an efficient method for collecting and retrieving archaeological data. With the help of geophysical surveys, hyperspectral data, aerial photographs, and high-resolution satellite imaging have successfully explored subsurface archaeological features over the Ve'szto-Ma'gor, Tell site in Hungary [13].

Similarly, archaeological sites in southeast Kansas were also studied using a geophysical approach [14]. They analyzed Lidar data for subsurface characteristics and variables affecting soil erosion in the Middle Neosho Watershed using Electrical Resistivity Tomography (ERT) and Normalized Difference Vegetation Index (NDVI). The authors believe that the technique and analysis strategy can be implemented to detect ancient crop markings based on identifying and examining soil erosion. On the other hand, data fusion methods such as "archaeo-geophysics," which may rapidly and non-invasively detect the locations and identities of buried ancient structures, are becoming increasingly sophisticated [15].

Supplementarily, Vegetation Indices derived from multispectral remote sensing data have been studied for their potential to be used in the detection of archaeological anomalies in ancient sites [12], [16–18]. Contrary to traditional remote sensing, which relies on several broadly defined spectral regions, multispectral remote sensing examines a number of precisely defined spectral channels. The use of multispectral sensors has been demonstrated for a variety of archaeological purposes, including the detection of crop stress [19–21], the differentiation of soil type and qualifying properties [22–24], the detection of chlorophyll vegetation [25–26], and the monitoring of water quality [27]. Archaeological features and their spectral signatures can be identified and determined by observing and interpreting vegetation health, i.e., spectral reflectance and proxy markers of monuments [28–30].

In Malaysia, the geophysical technique has been broadly applied in archaeology investigation. However, there is a limitation to studies utilizing the integration of both platforms. Moreover, there is no concrete indication, literature, or papers published associated with identifying specific spectra to detect the archaeological proxies in Malaysia. Hence, the study aims to validate the optimal spectral wavelength through spectra analysis by integrating aerial and ground platforms in identifying the archaeological proxies in Sungai Batu, Lembah Bujang.

2. Methods

2.1 Area of Interest

The Lembah Bujang is the territory of Kedah Tua, known as an ancient kingdom (Old Kedah). It is located in the northern region of the Malay Peninsula, as indicated in Figure 1. Extending a total of 144 square miles, the Muda River bounds it to the south, the Straits of Melaka to the east, the North-South Highway to the west, and the Bukit Choras to the north [31]. Geographically, the Lembah Bujang is situated near several notable features: mountains, barren hills, river valleys, and beaches [32]. The Merbok River and the Muda River nourish the Lembah Bujang. Mount Jerai, at 1300 meters in altitude, is the region's tallest peak; it is composed of shale rock and layers of mineral components, most notably quartzite [33]. Therefore, its strategic position was considered the hub of the entire archipelago. Lembah Bujang was an important administrative centre, economic hub, and port during its heyday. In the 1840s, Colonel James Low launched the archaeological research of Lembah Bujang [34]. However, FW Irby discovered the remnants of an ancient temple on Mount Jerai in 1894. The

ancient site of Lembah Bujang was the focus of this investigation. Several landowners and project developers discovered archaeological evidence associated with Lembah Bujang, a previously derelict woodland site in the Sungai Batu area. The CGAR team found signs of a sea or lake through a combination of transient electromagnetic (TEM) research and core drilling stratigraphy, as reported in [35].

The research also revealed that Sungai Batu was an important location as early as the first century CE. Only 52 of the 97 mounds planned for excavation at Sungai Batu were excavated. A total of five mounds were excavated between the years 2007 and 2010, with another fifteen mounds being uncovered in the years 2010 and 2011. Meanwhile, 32 mounds were dug during the study's second phase, which lasted from 2011 to 2021. The excavation discovered evidence of an iron smelting area (from the first century CE) and the remains of an ancient brick structure (*Candi*) from the second century CE. This finding is evidence of long-lost religious practices and rituals in the Lembah Bujang.

Moreover, the excavation team uncovered what is assumed to be a jetty, which included the remains of a roofed, tiled platform and brick platforms dating back to at least the 2nd century CE. In addition, the researchers discovered evidence of a *Syahbandar*, an administrative complex, and a warehouse area dating back to the sixth century BCE. Figure 1 depicts an overall aerial perspective of Sungai Batu.

Fig. 1. Aerial photography of the archaeological complex of Sungai Batu (close-up image) from the DJI P4-RTK Multispectral drone image captured in March 2021

2.2 Tools

2.2.1 SPOT-5 and SPOT -7 satellite dataset

This study utilizes high-resolution SPOT-5 and SPOT-7 multispectral satellite imagery. The multi-temporal satellite photos were acquired over the Sungai Batu section of the Lembah Bujang archaeological complex in March 2006 and November 2017. The image obtained by SPOT-5 in 2006 (ARSM) shows rugged terrain. It is also reported that no archaeological excavations were conducted in the Sungai Batu region in 2006. Additionally, data collected in 2017 (SPOT-7) and 2021 (DJI P4-RTK drone) was utilized to track how the archaeological excavation phase progressed, commencing in 2007. Thus, the evolution of the Sungai Batu excavation site is depicted in Figure 2. Table 1 details SPOT-5 and SPOT-7's respective features.

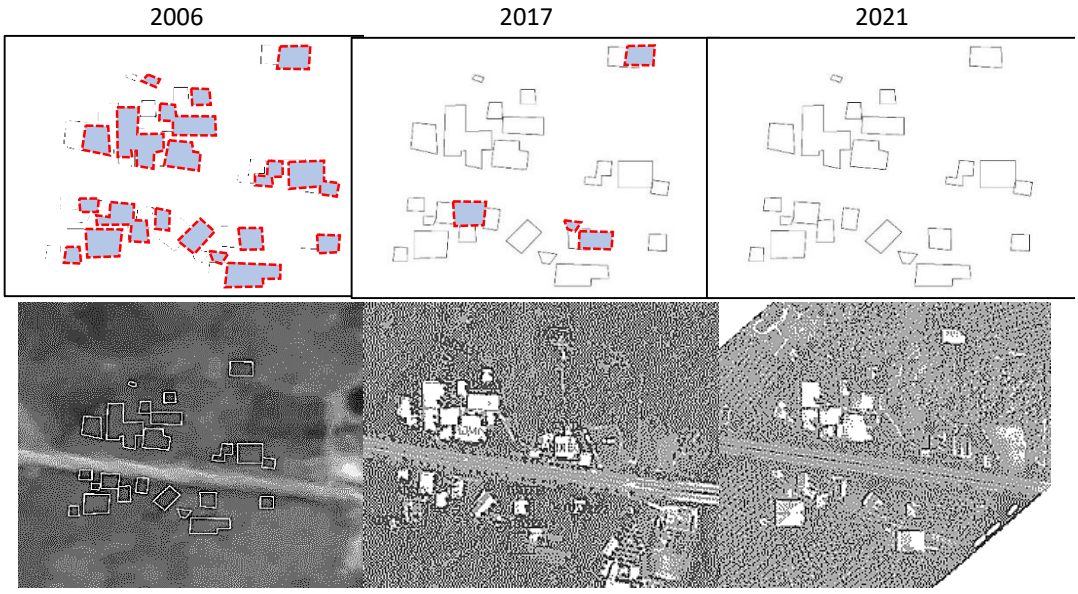

Fig. 2. Images showed the area of Sungai Batu (a) the red-dotted polygons indicated the invisible proxies (b) The SPOT-7 satellite image reveals that the region was being excavated and that several ancient sites had been unearthed and (c) the latest image of Sungai Batu in 2021 from a drone perspective

Table 1
The characteristics of SPOT-5 and SPOT-7 [36]

Platform	SPOT- 5 / SPOT-7
Characteristics	Same image swath of 60 km to maintain a high level of coverage capability Resolution with 1.5 m ortho imagery Addition of a blue band to get a native natural color image
Spatial resolution	Pan: 1.5m Multispectral: 6m Colour merge: 1.5m
Spectral Bands	Multispectral bands: Blue (450 nm – 525 nm) / (0.455 µm – 0.525 µm), Green (530 nm – 590 nm)/ (0.530 µm – 0.590 µm), Red (625 nm – 695 nm)/ (0.625 µm – 0.695 µm), Near-Infrared (760 nm – 890 nm)/ (0.760 µm – 0.890 µm) Panchromatic band: Panchromatic (450 nm – 745 nm),
Swath width	60 km (2 images) 120 km with single-pass mosaic
Geolocation	35 m without GCP; < 10 m with Ref3D

2.2.2 Geophysical-electrical resistivity thermography

In 2017, Electrical Resistivity Tomography (ERT) was performed in the dotted red square shown in Figure 3, depicting the compound area. Two-dimensional electrical resistivity tomography (ERT) was performed using a multichannel system and the ABEM Terrameter SAS4000 instrument, commonly utilized in environmental and archaeology research by the Geophysics Unit of Universiti Sains Malaysia. Besides, an academic open-source ERT software package known as Boundless

Electrical Resistivity Tomography (BERT) was used to carry out the 2D inversion technique, and irregular triangular meshes were utilized [15]. Table 2 summarizes the features of the ground geophysical (ERT) method used to locate underground features in Sungai Batu.

Fig. 3. The SPOT-7 satellite image captures the preliminary research region of Sungai Batu, Lembah Bujang. The red square box denotes the geophysical measuring area (electrical resistivity technique)

Table 2
The characteristic of Electric Resistivity Thermography (ERT) in identifying the subsurface features in Sungai Batu, Lembah Bujang [37]

Characteristic	Geophysical
Medium	Electrical Resistivity Thermography.
Year	2017
Accuracy	Depending on the method (Pole-pole < low accuracy) Pole-dipole > good accuracy) Dipole-dipole > high accuracy and detail profile)
Spectral Range	Electric wave
Spatial Extend	Several hectares (Vertical)
3D visualization	Available
Soil penetration	Available
Type information	Point

3. Solution Method and Algorithm

Based on the holistic scheme of the proposed technique depicted in Figure 4, the preliminary process comprises the following operation. Radiometric and atmospheric corrections and co-registration were applied during pre-processing to rectify the data. In order to conduct a more comprehensive analysis of vegetation, eight spectral indices were used. Each indication assists an archaeology detection analysis in its unique way, as in Table 3. Each indicator uses a different set of algorithms and constraints to expose different characteristics of the vegetation. Eight different groups of wavelength ranges were evaluated based on the spectral reflectance analysis results. These included the Archaeological Index (AI) [38], a Proposed Spectral 1 (PS-1), Proposed Spectral 2 (PS-2), and Proposed Spectral 3 (PS-3), additional spectral of ancient properties such as Iron, Granite, and Brick [39], as well as wavelengths Spectral studied by Sarris [13]. These bands were determined to be

optimal for plant growth by measuring their reflectance across a broad spectrum [26, 40, 41]. Measurements of Red and Near-Infrared reflectance are the basis for most Vegetation Index (VI) algorithms. Other indices' algorithms, such as GNDVI and EVI, use a Green and/or Blue color wavelength that is both an element of the spectrum and very Near-Infrared (NIR) [42, 43]. This is in contrast to what was mentioned previously.

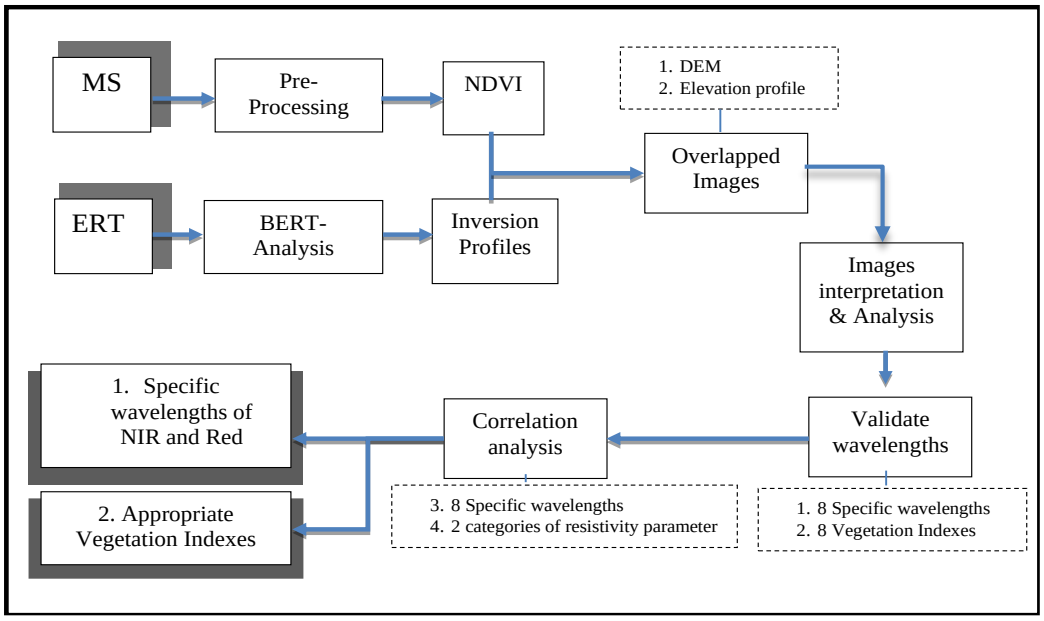

Fig. 4. Illustrative flow chart representation to validate the preliminary specific wavelength of archaeological proxies

Table 3
Indication of the calculation for determining the specific wavelengths between eight Vegetation Indexes and eight groups of selected spectral

	Wavelength	AI	PS-1	PS-2	PS-3	Iron	Granite	Brick	Sarris *et al.,*
	NIR	0.8	0.825	0.9	0.760	0.935	0.968	0.947	0.9
	Red	0.7	0.66	0.67	0.640	0.7	0.7	0.7	0.69
Algorithm									
NDVI									
GNDVI									
SR									
MSR									
DVI									
RDVI									
EVI									
MSAVI									

Next, the values of the spectra for each index and resistivity were averaged ($\underline{x}$) and ($\underline{y}$). Specifically, the *y* value was determined from the resistivity indicator's value range. Finally, the parameter values for *x* and *y* will be used to calculate the *R* values for each of the eight indices (NDVI, GNDVI, SR, MSR, DVI, RDVI, EVI, and MSAVI) against the Resistivity of the Ancient River (RAR) and resistivity of buried properties (RBP) were using the formula as in Eq. (1) and the result discussed in section result and discussion.

$$r = \frac{\Sigma(x-\underline{x})-(y-\underline{y})}{\sqrt{\Sigma(x-\underline{x})^2\Sigma(y-\underline{y})^2}} \quad (1)$$

3.1 New Method: Constant Experimental Evaluation

The "Constant Experimental Evaluation" (CEE) is developed further to emphasize the originality of the research. Based on the hypothesis, this technique seeks to answer whether NIR and RED wavelengths yield correct data, to begin with, or to what extent applying a new CEE method to these numbers improves their precision. In order to determine the optimal wavelengths, it is suggested that percentage increases and decreases should be used in an experimental setting. However, the maximum and minimum levels of the NIR and Red ranges must be considered when deciding on an increase or decrease in value. To overcome these limitations and achieve optimal results from the VIs algorithms, the existing linear regression technique must be modified by performing several calculations, with the percentage value indicating image optimization. The *r*-squared values derived from the spectral values will be generated afterwards via linear regression. Finally, the optimal spectral wavelength to detect the archaeological proxies in Sungai Batu will be obtaining new optimal wavelengths of NIR_{new} and Red_{new} with the improvement in accuracy value along with the percentage of image augmentation. The overall idea is illustrated in the flow chart below (see Figure 5).

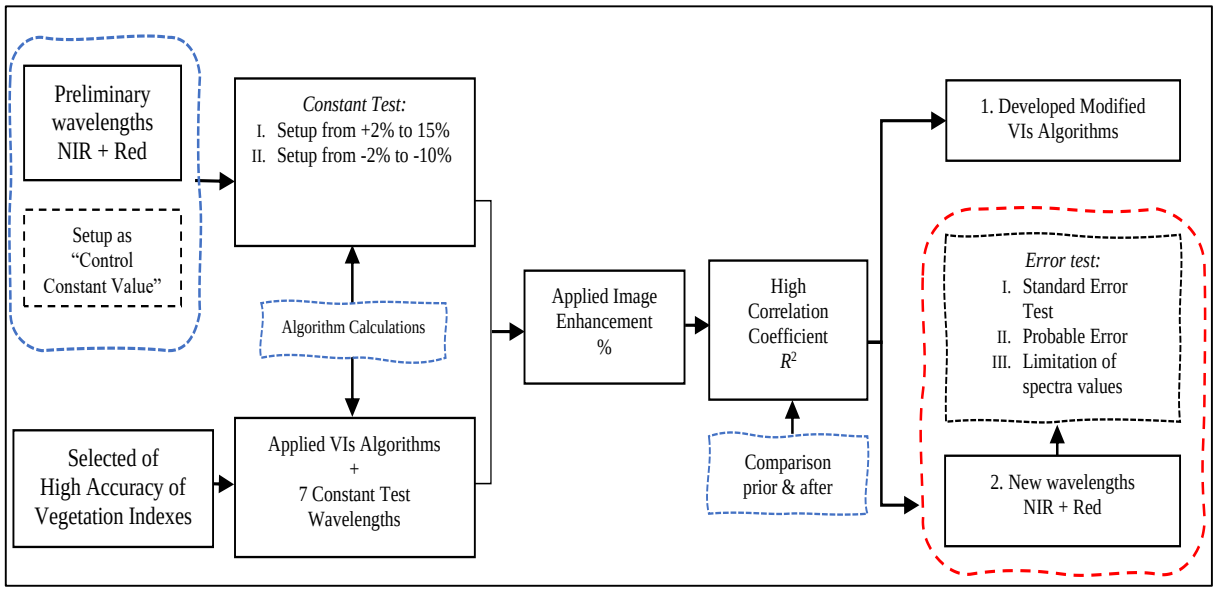

Fig. 5. Flowchart illustrating the validation of the particular wavelength of archaeological proxies using the CEE approach

4. Results and Discussion

4.1 Preliminary Optimal Spectral Wavelength

In order to figure out the relationship between spectral Vegetation Indexes (VIs) and ERTs and to confirm the preliminary specific wavelengths of proxies, statistical analysis was used. The correlation coefficient (*r*) was utilized to compare the different correlations between several VIs with a specific spectral wavelength of *ρ*NIR µm and *ρ*Red µm against the resistivity data. All indices, NDVI, GNDVI, SR, MSR, DVI, RDVI, EVI, and MSAVI, were then calculated as a mean value *($\bar{x}$).* Next, two separate resistivity data of Buried Properties (BRP) and Ancient River (RAR) were also calculated as a mean

value *($\bar{y}$)* for the r calculation. All BRP and RAR resistivity readings were purposefully selected from the resistivity indicator's range of values. The ranges of 1312.5 Ω-m to 3500 Ω-m and 21.25 Ω-m to 100 Ω-m are used as decision parameters for BRP and RAR, respectively. Table 4 displayed the comprehensive analysis for additional summative results. The median spectral results benchmark the preliminary wavelength values in determining the ideal spectral wavelengths. Therefore, the most significant spectral wavelength is Proposed Spectral 1 (PS-1), which ranges from NIR=0.825µm to Red=0.66µm and is relatively close to the median spectral result for each VIs sample.

Table 4
Result of the VI algorithms with a specific wavelength and spectral median of each index

Algorithms	Wavelength (nm)	AI (Agapiou *et al.,* 2012)	*PS- 1*	*PS- 2*	*PS- 3*	Iron	Granite	Brick	Sarris *et al.,* (2013)	Spectral Med.
	NIR	0.8	0.825	0.9	0.760	0.935	0.968	0.947	0.9	
	Red	0.7	0.66	0.67	0.640	0.7	0.7	0.7	0.69	
NDVI		0.067	0.111	0.146	0.086	0.144	0.161	0.150	0.132	0.125
GNDVI		0.19	0.2	0.241	0.16	0.26	0.275	0.265	0.24	0.229
SR		1.143	1.25	1.343	1.188	1.336	1.383	1.353	1.304	1.288
MSR		0.478	0.44	0.438	0.433	0.458	0.453	0.456	0.455	0.457
DVI		0.1	0.165	0.23	0.12	0.235	0.268	0.247	0.21	0.197
RDVI		0.082	0.135	0.184	0.10	0.184	0.208	0.193	0.167	0.156
EVI		0.448	1.01	1.06	1.33	0.77	0.84	0.8	0.789	0.881
MSAVI		3.35	-3.81	-4.44	-3.3	-4.64	-4.91	-4.73	-4.36	-4.193

Abbreviations: NDVI = Normalised Difference Vegetation Indices, **GNDVI** = Green Normalised Difference Vegetation Indices, **SR** = Simple Ratio, **MSR** = Modified Simple Ratio, **DVI** = Difference Vegetation Index, **RDVI** = Renormalized Difference Vegetation Index, **EVI** = Enhanced Vegetation Index**, MSAVI =** Modified Soil Adjusted Vegetation Index.

Subsequently, eight VIs algorithms were evaluated against two resistivity value ranges (RAR and BRP) to find out which Vegetation Indexes are associated (interrelated) with the ERTs data. The respective values of higher correlations were colored indicated as in (a) green: relatively strong positive correlation, (b) blue: relatively strong negative correlation, and (c) grey: relatively weak correlation.

Table 5 shows that the results show that almost all of the indices have a high correlation between VI algorithms and resistivity for RAR. The DVI and RDVI show a high positive correlation with RAR (*r = 0.94*) and RBP (*r = 0.95*). In identifying buried archaeological properties, MSAVI has a strong negative connection with RAR (*r* = -0.93) and RBP (*r* = -0.95). In contrast, NDVI for resistivity data over the (RAR) test had the lowest correlation with RAR (*r* = 0.66), indicating that the NDVI algorithm is less suited for detecting underground water than archaeologically buried structures or materials. Additional research [1], [44]–[45] confirms that the Normalized Difference Water Index (NDWI) algorithm is more successful when applied to water from the subsurface or underground. Thus, the study demonstrated that NDVI-RBP is more highly correlated (*r* = 0.95) than NDVI-RAR.

Table 5
Result of the correlation coefficient (*r*) with a range of -1 for each vegetation index and each type of resistivity data for the ancient river and buried properties

	NDVI	GNDVI	SR	MSR	DVI	RDVI	EVI	MSAVI	RAR	RBP
	0.067	0.19	1.143	0.478	0.1	0.082	0.448	-3.35	21.25	1312.5
	0.111	0.2	1.25	0.44	0.165	0.135	1.01	-3.81	32.5	1625
	0.146	0.241	1.343	0.438	0.23	0.184	1.06	-4.44	43.75	1937.5
	0.086	0.16	1.188	0.433	0.12	0.10	1.33	-3.3	55	2250
	0.144	0.26	1.336	0.458	0.235	0.184	0.77	-4.64	66.25	2562.5
	0.161	0.275	1.383	0.453	0.268	0.208	0.84	-4.91	77.5	2875
	0.150	0.265	1.353	0.456	0.247	0.193	0.8	-4.73	88.25	3187.5
	0.132	0.24	1.304	0.455	0.21	0.167	0.789	-4.36	100	3500
Mean	0.067	0.16	1.143	0.433	0.1	0.082	0.448	-4.91	1312.5	21.25
RARr	0.66	0.82	0.92	0.90	0.94	0.94	0.87	-0.93		
RBPr	0.95	0.94	0.93	0.92	0.95	0.95	0.88	-0.95		

Relative strong+ve correlation

Relative strong-ve correlation

Relative low correlation

Abbreviations: NDVI = Normalised Difference Vegetation Indices, **GNDVI** = Green Normalised Difference Vegetation Indices, **SR** = Simple Ratio, **rSR** = Reverse Simple Ratio, **MSR** = Modified Simple Ratio, **DVI** = Difference Vegetation Index, **RDVI** = Renormalized Difference Vegetation Index, **EVI =** Enhanced Vegetation Index**, MSAVI =** Modified Soil Adjusted Vegetation Index, **RAR** = Existing result of Resistivity; Ancient River, **RBP** = Existing result of Resistivity; Buried Properties.

4.2 Novelty of the CEE Method

Table 6 shows the initial spectral median correlation value (r) from the combination of (NDVI =0.111), (DVI=0.165), (RDVI=0.135), and (MSAVI=-3.81). Consequently, alterations were made to the four significant VIs algorithms using the CEE approach by continuously increasing and reducing percentages from the initial NIR=0.825 and Red=0.66 wavelength values. Furthermore, these initial wavelength values are referred to as "Control Constant Values" (as shown in the blue square box). The wavelengths that have a probability of achieving a "very strong" value of *R* more significant than the "Constant Control Value, *R* = 0.595," is determined by adding and subtracting constant percentages of 2%, 5%, 10%, and 15%, respectively. Since Red's peak spectral range is only 0.700µm, the maximum percentage increase is capped at 15%. However, due to the fact that the NIR minimum range is more than 0.760µm before approaching the Red-Edge wavelength zone, the maximum percentage reduction is set at 10%. Four percentage groups were analyzed for each method to discover which spectral wavelengths and percentages are optimal for recognizing archaeological characteristics and calculated as "Percentage Image Enhancement Values" (%IE). A sequence of percentages ranging from 20% through 50%, 80%, and 95% was used to compute the percentage.

Consequently, the CEE experiment test results demonstrated that the spectral wavelengths with decreasing values of -5% and 50% image enhancement had a greater R^2 value accuracy than the "control constant value" R^2 result, as given in Table 6, which is highlighted in the red square box. With the improved spectral wavelengths values of (NIR_{new}=0.783m) and (Red_{new}=0.627m) and the 50% of image enhancement, the linear regression graph, as presented in Figure 6, shows that the new value of R^2_{new} is 0.86, which is approximately higher than the previous value of (R^2=0.595). These significant values may be used as a future reference to determine archaeological proxies in Sungai Batu. The following Eq. (2) to Eq. (5) describe how this method improved pre-existing techniques across all four VIs. Lastly, *R* must be greater than six times the Probable Error (6*PEr*). Clearly, the *R*-value is greater than 6*PEr*, indicating a statistically significant correlation.

Modified Vegetation Indexes algorithms;

$$NDVI_{modified} = \frac{(NIR - RED)}{(NIR + RED)} x \frac{1}{2} \quad (2)$$

$$DVI_{modified} = \frac{(NIR - RED)}{2} \quad (3)$$

$$RDVI_{modified} = \frac{(NIR - RED)}{(NIR + RED)^{0.5}} x \frac{1}{2} \quad (4)$$

$$MSAVI_{modified} = \frac{2NIR+1\ [\,(2NIR+1)^2 - 8(NIR - RED)]^{0.5}}{4} \quad (5)$$

Lastly, the R^2 =0.86 value was tested with The Standard Error Test to cross-check the value of *R* is a significant correlation or low correlation.

Standard Error Test

n =28, R = 0.927

Here n is a total variable number of calculations as shown in Table 6, and *R* represents a value of R^2. Next, these values are calculated using Eq. (6), called Standard Error Test (*SEt*), followed by Probable Error Test (*PEt*), as shown in Eq. (7)-(8).

Standard error of R

$$SEr = s = \frac{(1-0.927^2)}{\sqrt{28}} = 0.026 \quad (6)$$

Probable Error

$$PEr = 0.6745 * \frac{(1-r^2)}{\sqrt{n}} \quad (7)$$

$$PEr = 0.0175$$

The limit of the spectral value of R;

$$R > 6PEr \quad (8)$$

$6PEr = 6\ (0.0175) = 0.105$ **= 0.927 > 0.105**

Table 6
Results using the method of "Constant Experiment Evaluation" (CEE) through four significant Vegetation Indexes and "Control Constant Value" of NIR and Red to validate the specific wavelengths in determining archaeological proxies

	NIR RED	% Image Enhancement (%IE)	NDVI * (%IE)	DVI * (%IE)	RDVI * (%IE)	MSAVI * (%IE)	R^2
Control constant	0.825 0.66	-	0.111	0.165	0.135	3.81	0.595
+15%	0.949 0.759	95	0.105	0.181	0.138	0.261	0.662
		80	0.088	0.152	0.116	0.22	0.661
		50	0.055	0.095	0.073	0.138	0.667
		20	0.022	0.038	0.029	0.055	0.661
+10	0.908 0.726	95	0.105	0.216	0.162	0.129	0.002
		80	0.089	0.182	0.140	0.109	0.003
		50	0.055	0.114	0.085	0.068	0.002
		20	0.022	0.046	0.034	0.027	0.001
+5%	0.866 0.693	95	0.105	0.164	0.132	0.126	0.027
		80	0.089	0.138	0.111	0.106	0.023
		50	0.055	0.865	0.069	0.067	0.060
		20	0.022	0.035	00.028	0.027	0.033
+2%	0.842 0.673	95	0.106	0.161	0.130	0.126	0.027
		80	0.090	0.135	0.110	0.106	0.025
		50	0.050	0.084	0.069	0.067	0.041
		20	0.022	0.034	0.027	0.027	0.044
-10%	0.756 0.594	95	0.105	0.142	0.119	0.073	0.353
		80	0.089	0.119	0.100	0.062	0.294
		50	0.055	0.075	0.063	0.039	0.278
		20	0.022	0.03	0.025	0.016	0.272
-5%	0.783 0.627	95	0.105	0.148	0.124	0.243	0.676
		80	0.089	0.125	0.105	0.205	0.677
		50	0.056	0.078	0.08	0.128	0.860
		20	0.022	0.031	0.026	0.051	0.672
-2%	0.809 0.647	95	0.105	0.154	0.744	0.247	0.1995
		80	0.089	0.130	0.626	0.208	0.200
		50	0.0555	0.081	0.392	0.130	0.200
		20	0.0222	0.032	0.157	0.052	0.199

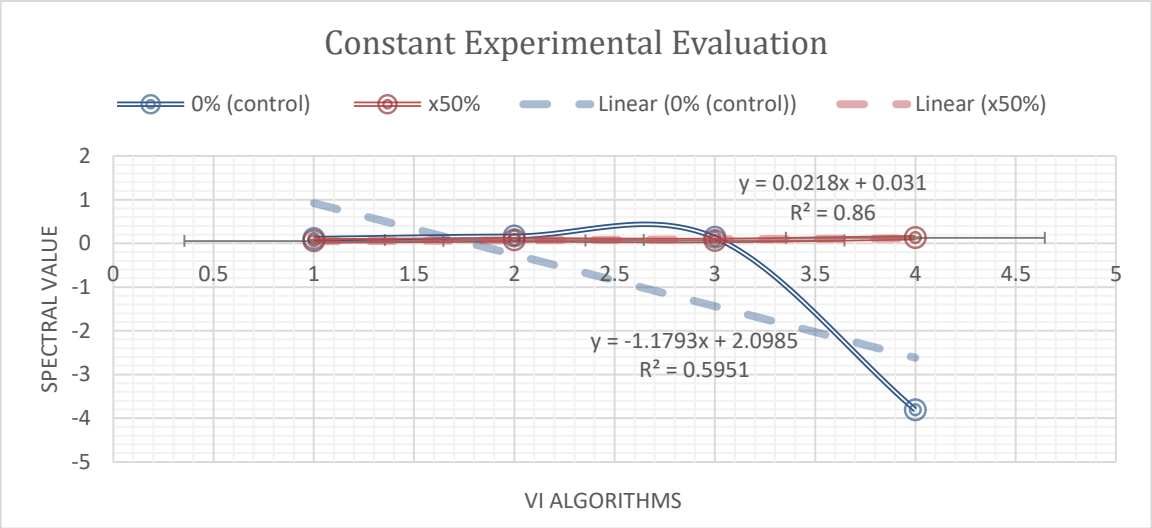

Fig. 6. Spectral plot of four VIs algorithms (NDVI, DVI, RDVI, and MSAVI) by comparing the R^2 values before and after applying the CEE method

5. Conclusions

In order to evaluate the appropriate spectral wavelengths for detecting archaeological proxies within the context of Malaysia's climate and vegetation heterogeneity, this research proposed a novel methodology by creating the "Constant Experimental Evaluation" (CEE) method. The first novel method used the Pearson correlation coefficient to validate the association between eight Vegetation Indices and Electrical Resistivity Thermography data measurements. The new CEE technique was then used to verify the preliminary results at particular wavelengths. According to the results of the first technique, the optimal spectral wavelengths are (NIR_{new}=0.783µm) and (Red_{new}=0.627µm), and 50% of image enhancement is achieved with an improvement in the correlation of 0.86 rather than 0.595. It has been found that the NDVI, DVI, RDVI, and MSAVI are the four Vegetation Indices that have the strongest correlation with the resistivity approach region. The remaining four suggested vegetation indices are moderately correlated. Future research will be expanded to determine the optimal spectral band and characterize the spectral patterns of the archaeological features, particularly in Malaysia's heterogeneous climate and vegetation.

Acknowledgement

This research was financially supported by the Universiti Teknologi Malaysia research grant under Vot. Number 09G38. The authors also would like to express their appreciation to the Geophysics Unit of the University of Sciences Malaysia (USM), the Centre of Global Archaeology Research, USM, and Mr Sheyh Sahibul Karamah Masnan for their cooperation. Also, the National Heritage Department of Malaysia and the Malaysia Remote Sensing Agency provided satellite information data for this research.

References

[1] Choi, Y. J., J. Lampel, S. Fiedler, D. Jordan, and T. Wagner. "A new method for the identification of archaeological soils by their spectral signatures in the vis-NIR region." *Journal of Archaeological Science: Reports* 33 (2020): 102553. https://doi.org/10.1016/j.jasrep.2020.102553

[2] Monna, Fabrice, Jérôme Magail, Tanguy Rolland, Nicolas Navarro, Josef Wilczek, Jamiyan-Ombo Gantulga, Yury Esin, Ludovic Granjon, Anne-Caroline Allard, and Carmela Chateau-Smith. "Machine learning for rapid mapping of archaeological structures made of dry stones–Example of burial monuments from the Khirgisuur culture, Mongolia–." *Journal of Cultural Heritage* 43 (2020): 118-128. https://doi.org/10.1016/j.culher.2020.01.002

[3] Roslan, Shairatul Akma, Fitri Yakub, Shuib Rambat, Norzailawati Mohd Noor, and Mokhtar Saidin. "The Integration of Aerial Sensing and Geophysical Techniques to Identify Buried Archaeological Properties in Sungai Batu, Bujang Valley." In *IOP Conference Series: Earth and Environmental Science*, vol. 540, no. 1, p. 012013. IOP Publishing, 2020. https://doi.org/10.1088/1755-1315/540/1/012013

[4] Roslan, Shairatul Akma, Fitri Yakub, Mokhtar Saidin, Shuib Rambat, Mohamed Attwa, and Mohd Zamzuri Ab Rashid. "A Comparative Assessment for the Archaeological Features Detection Using an Integration of Aerial Remote Sensing and Electrical Resistivity in Sungai Batu, Bujang Valley." *Journal of the Indian Society of Remote Sensing* 49 (2021): 2959-2975. https://doi.org/10.1007/s12524-021-01431-5

[5] Davis, Dylan S., Katherine E. Seeber, and Matthew C. Sanger. "Addressing the problem of disappearing cultural landscapes in archaeological research using multi-scalar survey." *The Journal of Island and Coastal Archaeology* 16, no. 2-4 (2021): 524-540. https://doi.org/10.1080/15564894.2020.1803457

[6] Jiménez-Brenes, Francisco Manuel, Francisca Lopez-Granados, Jorge Torres-Sánchez, José Manuel Peña, Pilar Ramírez, Isabel Luisa Castillejo-González, and Ana Isabel de Castro. "Automatic UAV-based detection of Cynodon dactylon for site-specific vineyard management." *PloS one* 14, no. 6 (2019): e0218132. https://doi.org/10.1371/journal.pone.0218132

[7] Polewski, Przemyslaw, Wei Yao, Lin Cao, and Sha Gao. "Marker-free coregistration of UAV and backpack LiDAR point clouds in forested areas." *ISPRS Journal of Photogrammetry and Remote Sensing* 147 (2019): 307-318. https://doi.org/10.1016/j.isprsjprs.2018.11.020

[8] Lasaponara, Rosa, and Nicola Masini. "Advances in remote sensing for archaeology and cultural heritage management." In *Proc. of I International EARSeL Workshop "Advances in Remote Sensing for Archaeology and Culturale Heritage Management", Rome*, vol. 30. 2008.

[9] Zhao, D. H., J. L. Li, and J. G. Qi. "Identification of red and NIR spectral regions and vegetative indices for discrimination of cotton nitrogen stress and growth stage." *Computers and Electronics in Agriculture* 48, no. 2 (2005): 155-169. https://doi.org/10.1016/j.compag.2005.03.003

[10] Lasaponara, Rosa, and Nicola Masini. "Satellite remote sensing in archaeology: Past, present and future perspectives." *Journal of Archaeological Science* 9, no. 38 (2011): 1995-2002. https://doi.org/10.1016/j.jas.2011.02.002

[11] Fenger-Nielsen, Rasmus, Jørgen Hollesen, Henning Matthiesen, Emil Alexander Sherman Andersen, Andreas Westergaard-Nielsen, Hans Harmsen, Anders Michelsen, and Bo Elberling. "Footprints from the past: The influence of past human activities on vegetation and soil across five archaeological sites in Greenland." *Science of the Total Environment* 654 (2019): 895-905. https://doi.org/10.1016/j.scitotenv.2018.11.018

[12] Agapiou, Athos, Vasiliki Lysandrou, Apostolos Sarris, Nikos Papadopoulos, and Diofantos G. Hadjimitsis. "Fusion of satellite multispectral images based on ground-penetrating radar (GPR) data for the investigation of buried concealed archaeological remains." *Geosciences* 7, no. 2 (2017): 40. https://doi.org/10.3390/geosciences7020040

[13] Sarris, Apostolos, Nikos Papadopoulos, Athos Agapiou, Maria Cristina Salvi, Diofantos G. Hadjimitsis, William A. Parkinson, Richard W. Yerkes, Attila Gyucha, and Paul R. Duffy. "Integration of geophysical surveys, ground hyperspectral measurements, aerial and satellite imagery for archaeological prospection of prehistoric sites: the case study of Vésztő-Mágor Tell, Hungary." *Journal of Archaeological Science* 40, no. 3 (2013): 1454-1470. https://doi.org/10.1016/j.jas.2012.11.001

[14] Maury, Shrikant, R. K. Tiwari, and S. Balaji. "Joint application of satellite remote sensing, ground penetrating radar (GPR) and resistivity techniques for targeting ground water in fractured Ophiolites of South Andaman Island, India." *Environmental Earth Sciences* 75 (2016): 1-21. https://doi.org/10.1007/s12665-015-5007-1

[15] Rizzo, Enzo, Alfonso Santoriello, Luigi Capozzoli, Gregory De Martino, Cristiano Benedetto De Vita, Daniela Musmeci, and Felice Perciante. "Geophysical survey and archaeological data at Masseria Grasso (Benevento, Italy)." *Surveys in Geophysics* 39 (2018): 1201-1217. https://doi.org/10.1007/s10712-018-9494-y

[16] Agapiou, Athos, Diofantos G. Hadjimitsis, Apostolos Sarris, Andreas Georgopoulos, and Dimitrios D. Alexakis. "Optimum temporal and spectral window for monitoring crop marks over archaeological remains in the Mediterranean region." *Journal of Archaeological Science* 40, no. 3 (2013): 1479-1492. https://doi.org/10.1016/j.jas.2012.10.036

[17] Mahdi, Ali M., Ahmed M. Eldosouky, Sayed O. El Khateeb, Ahmed M. Youssef, and Ahlam A. Saad. "Integration of remote sensing and geophysical data for the extraction of hydrothermal alteration zones and lineaments; Gabal Shilman basement area, Southeastern Desert, Egypt." *Journal of African Earth Sciences* 194 (2022): 104640. https://doi.org/10.1016/j.jafrearsci.2022.104640

[18] Rahimzadeganasl, Alireza, Ugur Alganci, and Cigdem Goksel. "An approach for the pan sharpening of very high resolution satellite images using a cielab color based component substitution algorithm." *Applied Sciences* 9, no. 23 (2019): 5234. https://doi.org/10.3390/app9235234

[19] Gupta, Ekta, Sonia Das, and M. B. Rajani. "Archaeological exploration in Srirangapatna and its environ through

remote sensing analysis." *Journal of the Indian Society of Remote Sensing* 45 (2017): 1057-1063. https://doi.org/10.1007/s12524-017-0659-9

[20] Beloev, Ivan H. "A review on current and emerging application possibilities for unmanned aerial vehicles." *Acta technologica agriculturae* 19, no. 3 (2016): 70-76. https://doi.org/10.1515/ata-2016-0015

[21] Melillos, George, Athos Agapiou, Kyriacos Themistocleous, Silas Michaelides, George Papadavid, and Diofantos G. Hadjimitsis. "Field spectroscopy for the detection of underground military structures." *European Journal of Remote Sensing* 52, no. 1 (2019): 385-399. https://doi.org/10.1080/22797254.2019.1625075

[22] Gennaro, Andrea, Alessio Candiano, Gabriele Fargione, Michele Mangiameli, and Giuseppe Mussumeci. "Multispectral remote sensing for post-dictive analysis of archaeological remains. A case study from Bronte (Sicily)." *Archaeological Prospection* 26, no. 4 (2019): 299-311. https://doi.org/10.1002/arp.1745

[23] Kirimi, Fridah, David Ndegwa Kuria, Frank Thonfeld, Esther Amler, Kenneth Mubea, Salome Misana, and Gunter Menz. "Influence of vegetation cover on the oh soil moisture retrieval model: a case study of the Malinda Wetland, Tanzania." (2016). https://doi.org/10.4236/ars.2016.51003

[24] Agapiou, Athos. "Enhancement of archaeological proxies at non-homogenous environments in Remotely Sensed Imagery." *Sustainability* 11, no. 12 (2019): 3339. https://doi.org/10.3390/su11123339

[25] Fuldain González, Juan José, []and Félix Rafael Varón Hernández. "NDVI identification and survey of a Roman road in the Northern Spanish province of Álava." *Remote Sensing* 11, no. 6 (2019): 725. https://doi.org/10.3390/rs11060725

[26] Díaz-Delgado, Ricardo, Gábor Ónodi, György Kröel-Dulay, and Miklós Kertész. "Enhancement of ecological field experimental research by means of UAV multispectral sensing." *Drones* 3, no. 1 (2019): 7. https://doi.org/10.3390/drones3010007

[27] Heggy, Essam, Jonathan Normand, Elizabeth M. Palmer, and Abotalib Z. Abotalib. "Exploring the nature of buried linear features in the Qatar peninsula: Archaeological and paleoclimatic implications." *ISPRS Journal of Photogrammetry and Remote Sensing* 183 (2022): 210-227. https://doi.org/10.1016/j.isprsjprs.2021.10.007

[28] Hussein, Nidal M., and Mohammed N. Assaf. "Multispectral remote sensing utilization for monitoring chlorophyll-a levels in inland water bodies in Jordan." *The Scientific World Journal* 2020 (2020). https://doi.org/10.1155/2020/5060969

[29] Luo, Lei, Xinyuan Wang, Huadong Guo, Rosa Lasaponara, Xin Zong, Nicola Masini, Guizhou Wang et al. "Airborne and spaceborne remote sensing for archaeological and cultural heritage applications: A review of the century (1907–2017)." *Remote sensing of environment* 232 (2019): 111280. https://doi.org/10.1016/j.rse.2019.111280

[30] Moriarty, Charles, Dave C. Cowley, Tom Wade, and Caroline J. Nichol. "Deploying multispectral remote sensing for multi-temporal analysis of archaeological crop stress at Ravenshall, Fife, Scotland." *Archaeological Prospection* 26, no. 1 (2019): 33-46. https://doi.org/10.1002/arp.1721

[31] Roslan, Shairatul Akma, Fitri Yakub, Mokhtar Saidin, Shuib Rambat, Mohamed Attwa, and Mohd Zamzuri Ab Rashid. "A Comparative Assessment for the Archaeological Features Detection Using an Integration of Aerial Remote Sensing and Electrical Resistivity in Sungai Batu, Bujang Valley." *Journal of the Indian Society of Remote Sensing* 49 (2021): 2959-2975. https://doi.org/10.1007/s12524-021-01431-5

[32] Taha, Adi Haji. "Archaeology in Peninsular Malaysia: Past, present and future." *Journal of Southeast Asian Studies* 18, no. 2 (1987): 205-211. https://doi.org/10.1017/S0022463400020506

[33] RAHMAN, NIK HASSAN SHUHAIMI BIN NIK ABD, and KAMARUDDIN BIN ZAKARIA. "Recent archaeological discoveries in Sungai Mas, Kuala Muda, Kedah." *Journal of the Malaysian Branch of the Royal Asiatic Society* 66, no. 2 (265 (1993): 73-80.

[34] Khoo, T. T. "Geomorphological evolution of the Merbok estuary area and its impact on the early state of Kedah, northwest peninsular Malaysia." *Journal of Southeast Asian Earth Sciences* 13, no. 3-5 (1996): 347-371. https://doi.org/10.1016/0743-9547(96)00042-6

[35] Mokhtar, Naizatul Akma, Mokhtar Saidin, and Jeffrey Abdullah. "The ancient iron smelting in Sg. Batu, Bujang valley, Kedah." In *Postgraduate student forum presentation, Chinese University of Hong Kong, China*. 2011.

[36] Agapiou, Athos, Diofantos G. Hadjimitsis, Andreas Georgopoulos, Apostolos Sarris, and Dimitrios D. Alexakis. "Towards an archaeological index: Identification of the spectral regions of stress vegetation due to buried archaeological remains." In *Progress in Cultural Heritage Preservation: 4th International Conference, EuroMed 2012, Limassol, Cyprus, October 29–November 3, 2012. Proceedings 4*, pp. 129-138. Springer Berlin Heidelberg, 2012. https://doi.org/10.1007/978-3-642-34234-9_13

[37] Roslan, Shairatul Akma, Noorzailawati Mohd Noor, Alias Abdullah, and Zuraini Md Ali. "Analysis of shrines properties using remote sensing approach: Case study of Lembah Bujang." *PLANNING MALAYSIA* 4 (2016). https://doi.org/10.21837/pm.v14i4.167

[38] Verhoeven, Geert, and Christopher Sevara. "Trying to break new ground in aerial archaeology." *Remote Sensing* 8, no. 11 (2016): 918. https://doi.org/10.3390/rs8110918

[39] Verhoeven, Geert, and Michael Doneus. "Balancing on the Borderline–a Low-cost Approach to Visualize the Red-edge Shift for the Benefit of Aerial Archaeology." *Archaeological Prospection* 18, no. 4 (2011): 267-278. https://doi.org/10.1002/arp.420

[40] Wueste, Elizabeth, Giulia Facchin, and Pier Matteo Barone. "Aventinus Minor Project: Remote Sensing for Archaeological Research in Rome (Italy)." *Remote Sensing* 14, no. 4 (2022): 959. https://doi.org/10.3390/rs14040959

[41] Gitelson, Anatoly A., and Mark N. Merzlyak. "Signature analysis of leaf reflectance spectra: algorithm development for remote sensing of chlorophyll." *Journal of plant physiology* 148, no. 3-4 (1996): 494-500. https://doi.org/10.1016/S0176-1617(96)80284-7

[42] Han, Haoshuang, Rongrong Wan, and Bing Li. "Estimating forest aboveground biomass using Gaofen-1 images, Sentinel-1 images, and machine learning algorithms: A case study of the Dabie Mountain Region, China." *Remote Sensing* 14, no. 1 (2021): 176. https://doi.org/10.3390/rs14010176

[43] Al Mansoori, Saeed, Alavi Kunhu, and Hussain Al Ahmad. "Automatic palm trees detection from multispectral UAV data using normalized difference vegetation index and circular Hough transform." In *High-Performance Computing in Geoscience and Remote Sensing VIII*, vol. 10792, pp. 11-19. SPIE, 2018. https://doi.org/10.1117/12.2325732